Zheng et al. BMC Pulmonary Medicine (2024) 24:545
https://doi.org/10.1186/s12890-024-03370-6

BMC Pulmonary Medicine

RESEARCH

Open Access

The diagnosis value of dual-energy computed tomography (DECT) multi-parameter imaging in lung adenocarcinoma and squamous cell carcinoma

Xingxing Zheng[1,2], Hongzhe Tian[1], Wei Li[1], Jun Li[3], Kai Xu[1], Chenwang Jin[2*] and Yuhui Pang[1*]

Abstract

Background Lung cancer continues to pose a serious risk to human health. With a high mortality rate, non-small cell lung cancer (NSCLC) is the major type of lung cancer, making up to 85% of all cases of lung cancer. Lung adenocarcinoma (AC), and lung squamous cell carcinoma (SC) are the two primary types of NSCLC. Determining the pathological type of NSCLC is important in establishing the most effective treatment method. Dual-energy computed tomography (DECT) multi-parameter imaging is an imaging technology that provides accurate and reliable disease diagnosis, and its uses are utilized for the combined diagnostic efficacy of AC and SC. The purpose of this study was to investigate the diagnostic value of spectral parameters of DECT in efficacy to AC and SC, and their combined diagnostic efficacy was also analyzed.

Methods We conducted a retrospective analysis of clinical and imaging data for 36 patients diagnosed with SC and 35 patients with AC. These patients underwent preoperative DECT chest scans, encompassing both arterial and venous phases, at our hospital from December 2020 to April 2022. The tumor diameter, water concentration (WC), iodine concentration (IC), normalized iodine concentration (NIC), Z effective (Zeff), and slope of the curve (*K*) in lesions were evaluated during two scanning phases in the two separate pathological types of lung cancers. The differences in parameters between these two types of lung cancers were statistically analyzed. In addition, receiver operating characteristic (ROC) curves were performed for these parameters to distinguish between SC and AC.

Results In a univariate analysis involving 71 lung cancer patients, the results from Zeff, IC, NIC, and K from the AC's arterial and venous phase images were more elevated than those from the SC ($P < 0.05$). In contrast, the WC results were lower than those from SC ($P < 0.05$). The area under the ROC curve (AUC) for multi-parameter joint prediction typing was 0.831, with a corresponding sensitivity of 63.9% and specificity of 94.3%.

*Correspondence:
Chenwang Jin
jinchenwang202406@163.com
Yuhui Pang
pangyuhui1994@163.com
Full list of author information is available at the end of the article

Conclusion It is possible to distinguish between central SC and AC using the spectrum characteristics of DECT-enhanced scanning (Zeff, IC, NIC, K, WC, and tumor diameter). Diagnostic effectiveness can be greatly improved when multiple variables are included.

Keywords Energy spectrum CT, Lung adenocarcinoma, Lung squamous cell carcinoma

Background

Lung cancer is one of the world's most prevalent and a major contributor to cancer-related mortality [1, 2]. The most pervasive pathological forms of lung cancer are lung adenocarcinoma (AC) and squamous cell carcinoma (SC), and each has a unique therapeutic treatment strategy, with notable variations in chemotherapy regimens [3–5]. The identification of the pathological type of lung cancer before beginning therapy might therefore aid in the development of precise treatment strategies and prognostication. The majority of pathological diagnoses of lung cancer currently depend on cytological analysis, fiberoptic bronchoscopy, or fine needle aspiration biopsy [6]. Certain tumors, particularly those located deep within the lung tissue or near major blood vessels and bones, can be challenging to obtain a tissue sample from due to their anatomical position. This makes biopsy procedures more complex and potentially risky, thus rendering the above methods unsuitable [7]. A non-invasive, safe, and economical technique is an essential tool to assist in identifying the histological type of malignancies.

At present, conventional Computed tomography (CT) is a commonly used method for diagnosing lung cancer, but due to the beam hardening effect caused by mixed energy X-rays, it can affect the accuracy of CT value measurement and easily lead to misdiagnosis or missed diagnosis [8, 9]. The PET-CT can not only determine the exact location of lesions, but also measure tumor metabolic activity, but these modalities are associated with excessive radiation doses and high costs [10]. MRI have been used to detect lesions in lung in recent years, but the bad effect of faint signals and breathing motion artifacts need to overcome [11, 12]. Various pathological types of lung cancer exhibit distinct biological behaviors and pathological features and therefore require effective and sensitive modalities for diagnosis.

Dual-energy CT (DECT) significantly increases the precision and reliability of disease diagnosis by not only offering images of anatomical morphology but also enabling the conversion of single-parameter diagnostic modes to multi-parameter diagnostic modes [7, 13]. Furthermore, it can reveal additional biological details about lesions and differentiate between various tissue components [14–17]. Fehrenbach et al. [18]considered that only standardized iodine concentration (NIC) in the arterial phase (AP) was significant for the differential diagnosis of NSCLC. In contrast, Li et al. [19]showed that venous phase (VP) of IC can differentiate SC from AC by reflecting tumor microvessel density. Problems, such as single-phase scanning and single spectral parameters, have caused a lot of controversies. This study improves the above issues. This study aims to explore the diagnostic value of DECT parameters in distinguishing AC and SC diagnosis, and analyze their combined diagnostic efficacy.

Methods

Patients

The Ethics Committee of Shaanxi Province's Baoji Central Hospital approved this study, and the experimental protocol was executed according to the approved guidelines. Informed permission was waived in view of the study's retrospective nature. Seventy-one patients with pathologically confirmed AC and SC who had preoperative energy spectrum CT chest scans performed at the Baoji Central Hospital in Shaanxi Province between December 2020 and April 2022 had their clinical and imaging data retrospectively analyzed. There were 35 cases of AC and 36 cases of SC, of whom 34 were males and 37 were females. Inclusion criteria: (1) Preoperative chest energy spectrum CT scan was performed, and the CT image could clearly display the lesion; (2) Pathological confirmation of non-small cell lung cancer through puncture biopsy, fiberoptic bronchoscopy, or surgical resection. Exclusion criteria: (1) Acceptance of radiation and chemotherapy before CT examination or biopsy, fiberoptic bronchoscopy, or surgical resection; (2) Missing or incomplete imaging and clinical data; (3) Cases where the lesion was too small or had too much liquefaction necrosis; (4) Cases where the lesion was not clearly displayed due to obstructive atelectasis, pneumonia, pleural effusion, etc. Figure 1 illustrates the flow diagram of the presentation study.

CT examination

Plain and three-phase enhanced scans using 256-row single source dual energy CT (GE, Revolution CT Xstream Edition) were performed. The scanning range spanned from the apex of the lungs to the lower edge of the liver. The gemstone spectral imaging (GSI) mode was adopted. The parameters of the conventional sequence included instantaneous switching of tube voltage between 80 kVp and 140 kVp, tube current of 200–400 mA, layer thickness and spacing of 5 mm, reconstruction layer thickness of 1.25 mm, detector width of 80 mm, tube rotation time of 0.5 s, pitch of 0.992:1, FOV of 35 cmx35 cm. The

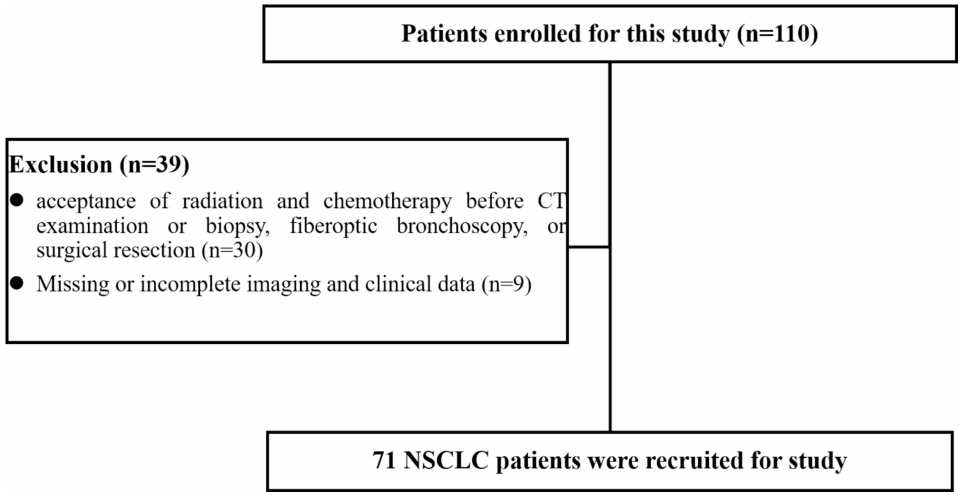

Fig. 1 Flowchart for the inclusion and exclusion of patients

contrast agent for enhanced scanning was iodohexanol (300 mgI/mL, dose of 1.2 mL/kg body mass), injected through the anterior elbow vein at a rate of 3.0-3.5 mL/s. Arterial (AP), venous (VP), and delayed phase images were obtained after contrast agent injection for 30 s, 60 s, and 120 s, respectively.

Imaging analysis

Scanned and reconstructed data was transferred to the post-processing workstation (GE, AW 4.6), and arterial and venous phase images were generated using GSI Viewer analysis software. Dual-energy datasets for arterial and venous phases for post-processing were selected. Select three consecutive image slices containing the maximum cross-section of the tumor and adjacent upper and lower levels for measurement; Manually draw a circular or elliptical region of interest (ROI) as large as possible (close to half to two-thirds of the lesion area), avoiding the edges, blood vessels, calcification, and necrotic areas of the tumor. The measurement methods and parameters for arterial and venous lesions are consistent.

Quantitative parameter measurement included: (1) The calculation of the slope of the energy spectrum attenuation curve (k)=(HU40keV HU100keV)/(100−40); (2) Effective ordinal number (Zeff); (3) The measurement of the iodine concentration (IC) of arterial phase lesions and the iodine value of the aorta at the same level as the lesion using Iodine substance map, and the calculation of the standardized iodine concentration (NIC). The standardized iodine concentration is equal to the iodine value of the lesion/the iodine value of the aorta at the same level. (4) Measurement of the water concentration (WC). (5) Measurement of the maximum thickness of the largest layer of the lesion axis map (measured sample thickness in this study).

Histochemical examination

A pathologist with ten years of expertise in immunohistochemical staining examined tumor specimens. The pathologist numbered, assessed, and documented each section's pathological nature without having access to clinical data or spectral CT scan results. The World Health Organization Classification of Lung Tumors was followed in the application of the histopathological criteria for diagnosis.

Statistical analysis

SPSS 25.0 was used to perform statistical analysis. The classification count data was reported as a percentage of the total number of cases, and $\chi 2$ test was used to compare the two groups.

The measurement data undergoing normality testing and data that followed a normal distribution were presented as mean ± standard deviation (±SD). To compare the two groups, two independent sample t-tests were employed. The median (quartile) was used for presenting data that did not fit into a normal distribution, and the Mann-Whitney U test was used to compare the two groups. Logistic regression was used to integrate the spectral CT parameters with statistically significant differences between the two groups based on the weighting coefficient, and the diagnostic efficacy of quantitative parameters was analyzed using ROC curves. A P-value of <0.05 indicates a statistically significant difference.

Results

Clinical data and routine imaging data of patients

The findings from the study showed that the clinical characteristics of the two patient groups—including age, gender, and smoking history—did not differ statistically significantly ($P>0.05$). The maximum diameter of squamous cell carcinoma was larger than that of

Table 1 Summary of clinical and routine imaging data

Characteristics	AC ($n=35$)	SC ($n=36$)	P-value
Age (years)	65.71 ± 10.44	64.19 ± 7.06	0.476
Gender			0.901
Female	19 (54)	18 (50)	
Male	16 (46)	18 (50)	
Smoking history			0.921
No	15 (43)	14 (39)	
Yes	20 (57)	22 (61)	
Speculation sign			0.118
No	12 (34)	20 (56)	
Yes	23 (66)	16 (44)	
Lobulation sign			0.478
No	3 (9)	6 (17)	
Yes	32 (91)	30 (83)	
Pleural indentation			0.188
No	13 (37)	20 (56)	
Yes	22 (63)	16 (44)	
Tumor size (cm)	2.8 (2.05, 4.05)	5 (3.5, 6.62)	< 0.001*
Tumor location			0.138
Right upper lobe	16 (46)	7 (19)	
Right lower lobe	6 (17)	11 (31)	
Right middle lobe	0 (0)	1 (3)	
Left upper lobe	8 (23)	10 (28)	
Left lower lobe	5 (14)	7 (19)	

*$P<0.05$

adenocarcinoma [5 (3.5, 6.62) cm and 2.8 (2.05, 4.05) cm, $P<0.05$]. However, there was no statistically significant difference ($P>0.05$) in the comparison of conventional imaging features such as hair prick sign, lobulation sign, pleural traction, and tumor location. Table 1 illustrates the clinical data.

Comparison of CT parameters of different energy spectra between AC and SC groups

As shown in Tables 2 and 3; Figs. 2 and 3, the Zeff, IC, NIC, and K obtained from AP and VP images in the AC patients were all higher than those in SC patients ($P<0.05$), whereas the WC was comparatively lower than that in SC ($P<0.05$).

ROC curve analysis and display of diagnostic efficiency of spectral CT parameters

Logistic regression was used to integrate the spectral CT parameters with statistically significant differences between the two groups based on the weighting coefficient, as seen in Table 4; Fig. 4. The regression model was:11.465−3.727*VP_(Intercept) + 0.014*VP_Zeff-0.19*VP_water base value + 10.275*VP_IC-1.875*VP_NIC-0.112*VP_K + 0.004*AP_Zeff + 0.042* AP_water base value −16.286* AP_ IC + 3.028* AP_NIC + 0.318* AP_K-3.727* tumor diameter. The AUC of the ROC curve was 0.831, with sensitivity of 63.9% and specificity of 94.3%.

Discussion

The histological classification of lung cancer has been proven to be an independent prognostic indicator. Due to significant differences in biological behavior, treatment strategies, and prognosis evaluation among different pathological subtypes of lung cancer, AC and SC are the two main types of NSCLC. Determining the pathological type of NSCLC is crucial for establishing the most effective treatment methods [4, 20]. Therefore, the treatment methods for lung cancer patients with different pathological subtypes have certain reference value, which can help reduce mortality, prolong survival time, and improve quality of life.

In addition to identifying and classifying tumor disorders based on their physical features, DECT can also provide insight into the underlying biology of the tumor by analyzing its various stages [13, 21–23]. Although the parameters of VP were left out of the study, Wang et al. [20] demonstrated the diagnostic value of the spectral curve slope of 40 to 70 kev in the AP-K and IC in

Table 2 Comparison of energy spectrum parameters in arterial phase of CT enhanced scanning between lung adenocarcinoma and squamous cell carcinoma patients

Group	Zeff	WC	IC	NIC	K
AC	8.53 (8.2, 8.73)	1023.20 (1009, 1029.78)	15.70 (9.56, 20.53)	0.16 (0.11, 0.2)	1.76 (1.1, 2.42)
SC	8.25 (7.98, 8.43)	1027.84 (1023.83, 1033.75)	10.52 (6.4, 13.6)	0.13 (0.08, 0.16)	1.27 (0.75, 1.7)
P-value	<0.01*	0.03*	<0.01*	0.05*	0.01*

*$P<0.05$. AC: adenocarcinoma; SC: Squamous cell carcinoma; WC: water concentration; IC: iodine concentration; NIC: normalized iodine concentration; Zeff: Z effective; K: slope of the curve

Table 3 Comparison of energy spectrum parameters in venous phase of CT enhanced scanning between lung adenocarcinoma and squamous cell carcinoma patients

Group	Zeff	WC	IC	NIC	K
AC	8.53 ± 0.35	1023.60 (1014.26, 1029.65)	15.77 ± 6.13	0.41 (0.32, 0.52)	1.84 ± 0.71
SC	8.23 ± 0.31	1029.28(1024.18, 1033.75)	11.05 ± 5.83	0.34 (0.2, 0.47)	1.24 ± 0.59
P-value	<0.01	0.02	<0.01	0.03	<0.01

*$P<0.05$. AC: adenocarcinoma; SC: Squamous cell carcinoma; WC: water concentration; IC: iodine concentration; NIC: normalized iodine concentration; Zeff: Z effective; K: slope of the curve

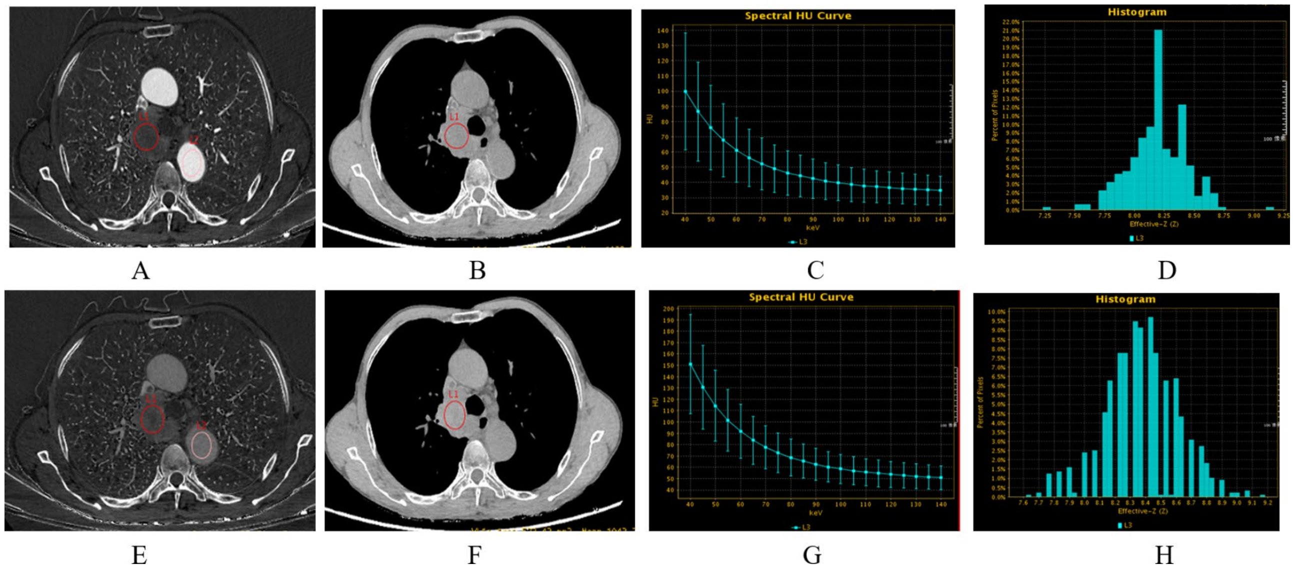

Fig. 2 (1) Quantitative parameters of arterial (**A**-**D**) and venous phases (**E**-**H**) in 70 year old male patients with AC. Iodine concentration images (**A**, **E**); Water concentration mages (**B**, **F**); Slope of the curve (**C**, **G**); Z effective images (**D**, **H**); In the arterial phase, IC, NIC, WC, K and Zeff are 11.38, 0.15, 1029.72, 1.32 and 8.19. In the venous phase, IC, NIC, WC, K and Zeff are 12.38, 0.40, 1033.56, 1.53 and 8.38

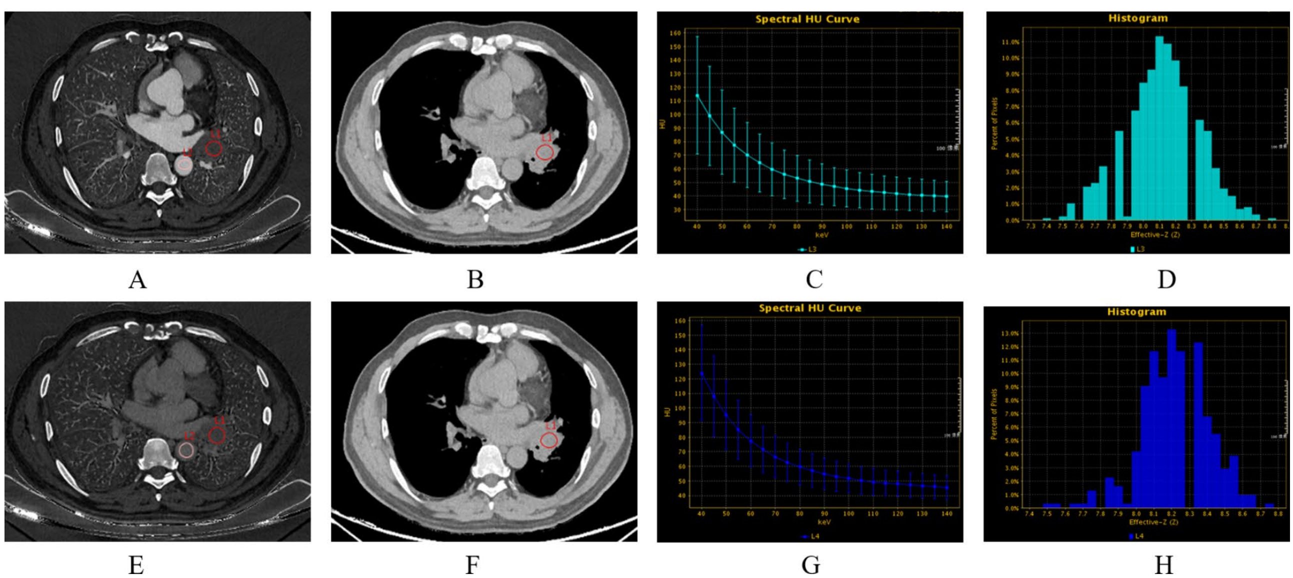

Fig. 3 (1) Quantitative parameters of arterial (**A**-**D**) and venous phases (**E**-**H**) in 61 year old male patients with SC. Iodine concentration images (**A**, **E**); Water concentration mages (**B**, **F**); Slope of the curve (**C**, **G**); Z effective images (**D**, **H**); In the arterial phase, IC, NIC, WC, K and Zeff are 10.66, 0.12, 1034.50, 1.15 and 8.13. In the venous phase, IC, NIC, WC, K and Zeff are 11.06, 0.30, 1040.17, 1.20 and 8.22. (WC: water concentration, IC: iodine concentration, NIC: normalized iodine concentration, Zeff: Z effective; K: slope of the curve)

distinguishing between SC and AC. By expressing tumor microvessel density, on the other hand, Li [19] demonstrated that VP-IC can distinguish between SC and AC by utilizing dual-energy spectral CT scanning technology to investigate the function of dual-phase scanning in lung cancer subtypes, the problems above were addressed, and improved.

Comparison of spectral CT quantitative parameters between AC and SC

The term "energy spectrum curve" describes the curve that shows how the energy level of an X-ray affects the CT value of various lesions or tissues. The chemical molecular structure of different substances will change, and different molecules will attenuate energy differently [24]. Therefore, subgroups of lung cancer can be identified using the K of the energy spectrum curve. According to the research both domestically and internationally,

Table 4 Performance indicators of arterial and venous phase DECT parameters and their combined predictive classification

Parameter	AUC	Sensitivity (%)	Specificity (%)	Threshold	95% CI
AP					
Zeff	0.70	0.861	0.514	8.525	0.577 ~ 0.823
WC(mg/cm^3)	0.65	0.639	0.657	1026.305	0.517 ~ 0.78
IC(mg/cm^3)	0.70	0.806	0.571	14.475	0.565 ~ 0.815
NIC(mg/cm^3)	0.64	0.778	0.514	0.162	0.506 ~ 0.766
K	0.68	0.750	0.571	1.698	0.549 ~ 0.802
VP					
Zeff	0.70	0.861	0.514	8.525	0.577 ~ 0.823
WC(mg/cm^3)	0.65	0.639	0.657	1026.305	0.517 ~ 0.780
IC(mg/cm^3)	0.69	0.806	0.571	14.475	0.565 ~ 0.815
NIC(mg/cm^3)	0.64	0.778	0.514	0.162	0.506 ~ 0.766
K	0.68	0.75	0.571	1.698	0.549 ~ 0.802
Tumor size	0.73	0.694	0.743	3.95	0.605 ~ 0.853
Combined diagnosis	0.83	0.639	0.943	0.60	0.736 ~ 0.926

*$P < 0.05$. AC: adenocarcinoma; SC: Squamous cell carcinoma; AP: Arterial phase; VP: venous phase. WC: water concentration, IC: iodine concentration, NIC: normalized iodine concentration, Zeff: Z effective; *K*: slope of the curve

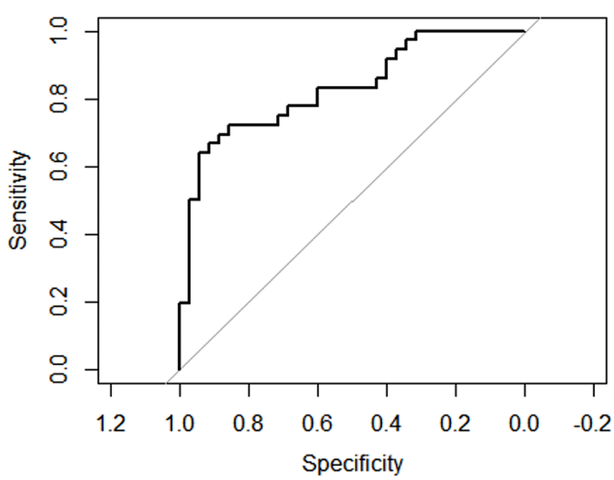

Fig. 4 Identification of ROC curves between lung adenocarcinoma and squamous cell carcinoma using combined energy spectrum CT parameters

the K value of AC was greater than that of SC [25]. This could be connected to the different material makeup or metabolic processes of lung cancer. However, the single energy node of K in this study is not completely consistent with that in the study of Zhang et al. [7]. The single energy nodes of K in Zhang's study are 40 keV and 110 keV; however, in this investigation, the CT values in the single energy 40 ~ 100 keV between the two groups are significantly different, leading to the final selection of 40 keV and 100 keV as the single energy nodes of K. In this investigation, the Zeff, IC value, and NIC value were successfully measured in addition to the CT value of any level within the 40–190 keV range using the software. The Zeff is the atomic number of elements with the same decay coefficient as compounds or mixtures, which can be utilized to determine the tissue composition of substances, particularly in substances with the same CT values. It is a quantitative index comprising many substances [26, 27]. The values of Zeff, IC, and NIC were measured in addition to obtaining the CT value of any level in the 40–190 keV range. The findings from our study indicated that the Zeff of AC was higher than that of SC. This difference may be caused by the primary characteristics of AC, which include unclear cell boundaries, solid blocks or strips, and a tendency to form an adenoid structure supported by a fibrous matrix and secreting mucus. Whereas, the internal structure of SC is closely arranged and exhibits the formation of keratinization and keratinized beads (also known as cancer beads) and a unique intercellular bridge structure. The two have different Zeff because of their differing chemical composition and densities [28]. Comparatively, adenocarcinoma grows in diversification, with rich stroma, relatively few tumor cells per unit volume, and low water content; as a result, its water content (WC) was lower than that of SC. Most SC, on the other hand, grows in aggregation, with more tumor cells per unit volume and greater water content. These results were confirmed by a pathological study conducted by Zhong et al. [29], where 50 cancer patients (including 35 cases of adenocarcinoma and 22 cases of squamous cell carcinoma) were analyzed. The study found that the Zeff (7.90 ± 0.14) and IC of AC were higher than those of SC, while the WC in AC was substantially lower compared to that in SC. The findings of this investigation align with the findings of other researchers.

The quantitative analysis of iodine content reflects the intravascular blood flow distribution and vascular status. However, many factors influence it, including the patient's cardiac output and blood volume, the concentration and flow rate of the contrast agent, and the injection dose and rate. The NIC is the ratio of tumor IC to aortic or subclavian artery IC at the same level.

According to various studies, NIC can reduce the effect of variations in individual circulation variability in the iodine content of tumors, improving the accuracy of the lesions' blood supply. The sources of tissue vary among clinical forms of lung cancer, and iodine concentrations are influenced by tumor angiogenesis [30, 31]. During growth, SC has a relatively weak internal blood supply and expand slowly, whereas AC tends to form an abundance of ethmoid capillaries [32]. Thus, following increased scanning, the iodine concentration of AC was higher than that of SC, which was in line with Zhong's findings. Furthermore, this study found that IC and NIC in VP were higher than those in AP, which may be due to the fact that the contrast agent in AP was not filled with microvessels, while the contrast agent in VP was filled with microvessels and penetrated the basement membrane into the intercellular space. For spectral CT scanning, Mu et al. [25] collected 127 patients with pulmonary AC and 70 patients with pulmonary SC verified by histology. According to the study, vein IC and NIC were higher than arterial phase NIC, and the spectrum parameters of AC were increased compared to those of SC. These parameters may offer a specific benchmark for the categorization of lung cancer. Nonetheless, we discovered that IC was more effective in AP and VP than NIC when comparing AC to SC, which was in line with Li et al.'s findings [19]. This suggests that NIC is dependent on the degree of lesion and aortic enhancement and that NIC deviation may result from changes in aortic diameter.

Study on the efficacy of quantitative parameters in differentiating AC from SC

A ROC curve was drawn to assess the value of the single parameter index and joint prediction of lung cancer categorization according to the findings of the quantitative parameter analysis. In this study, the AUC of the ROC curve predicted by a single parameter was 0.65–0.73. This indicated that when only a certain spectral quantitative parameter of lung cancer is considered, its evaluation value is limited in most cases. To increase prediction efficiency, this study will jointly analyze meaningful quantitative parameters while carefully taking into account the distribution characteristics of iodine concentration and tumor heterogeneity. The findings of this investigation showed that the AUC of the ROC curve was 0.83 when multiple quantitative parameters were combined. This indicates a potential clinical application and significantly raises the prediction accuracy of lung cancer subtypes.

Limitations and prospects of the study

This study has the following limitations: (1) A small sample size; thus, a larger number of subjects in future research for more robust validation is required. (2) Research indicates that the synergistic application of PET/CT and spectral CT can leverage their respective strengths, thereby enhancing the diagnostic accuracy for lung diseases, this should be explored in future research [33, 34]. Additional research is required to verify the model across a larger number of cases and to compare it with PET/CT characteristics. (3) The relationship between lung cancer classification and prognosis, as well as the influence of various classifications on patient outcomes, is significant. Currently, the subtypes identified are SC and AC. Further investigation is required into small cell lung cancer and less common subtypes, including large cell carcinoma.

In conclusion, the quantitative examination of spectral CT parameters was determined to be useful in identifying lung cancer subtypes and offers important information for assessing prognosis and clinical treatment options. For future studies, the sample size will be extended, examine more pathological types will be examined, and the research will be applied to tumors in other organs and diseases.

Abbreviations

CT	computed tomography
AC	adenocarcinoma
SC	Squamous cell carcinoma
AP	Arterial phase
VP	venous phase
WC	water concentration
IC	iodine concentration
NIC	normalized iodine concentration
Zeff	Z effective
K	slope of the curve

Acknowledgements
Not applicable.

Author contributions
XXZ: Data curation, Methodology, Writing - original draft, Software, Investigation. YHP: Data curation, Methodology , Software, Investigation. HZT and JL: Visualization, Investigation. WL: Software, Formal analysis. KX: Visualization, Investigation. CWJ and YHP: Conceptualization, Methodology, Writing - review & editing. All authors revised the report and approved the final version before submission.

Funding
This work was supported by the Baoji Health Committee Foundation of China (Grant Number 2021-023, Grant Number 2024-035, Grant Number 2019-01).

Data availability
The datasets during and/or analyzed during the current study available from the corresponding author on reasonable request.

Declarations

Ethics approval and consent to participate
Our study followed the Declaration of Helsinki and it was approved by the Ethics Committee of the Baoji Central Hospital (No. BZYL2022-14) and the requirement for informed consent from the patients was waived.

Consent for publication
Not applicable.

Competing interests

The authors declare no competing interests.

Author details

[1]Department of Medical Imaging, Baoji Central Hospital, Baoji, China
[2]Department of Medical Imaging, First Affiliated Hospital of Xi'an Jiaotong University, Xi'an, China
[3]Department of Pathology, Baoji Central Hospital, Baoji, China

Received: 16 June 2024 / Accepted: 28 October 2024
Published online: 30 October 2024

References

1. Rami-Porta R, Bolejack V, Crowley J, Ball D, Kim J, Lyons G, Rice T, Suzuki K, Thomas CF Jr., Travis WD, Wu YL, Staging I, Prognostic Factors Committee AB, Participating I. The IASLC Lung Cancer Staging Project: proposals for the revisions of the T descriptors in the Forthcoming Eighth Edition of the TNM classification for Lung Cancer. J Thorac Oncol. 2015;10(7):990–1003.
2. Zheng RS, Chen R, Han BF, Wang SM, Li L, Sun KX, Zeng HM, Wei WW, He J. [Cancer incidence and mortality in China, 2022]. Zhonghua Zhong Liu Za Zhi. 2024;46(3):221–31.
3. Allemani C, Matsuda T, Di Carlo V, Harewood R, Matz M, Niksic M, Bonaventure A, Valkov M, Johnson CJ, Esteve J, Ogunbiyi OJ, Azevedo ESG, Chen WQ, Eser S, Engholm G, Stiller CA, Monnereau A, Woods RR, Visser O, Lim GH, Aitken J, Weir HK, Coleman MP, Group CW. Global surveillance of trends in cancer survival 2000-14 (CONCORD-3): analysis of individual records for 37 513 025 patients diagnosed with one of 18 cancers from 322 population-based registries in 71 countries. Lancet. 2018;391(10125):1023–75.
4. Qi Y, Yang L, Liu B, Liu L, Liu Y, Zheng Q, Liu D, Luo J. Highly accurate diagnosis of lung adenocarcinoma and squamous cell carcinoma tissues by deep learning. Spectrochim Acta Mol Biomol Spectrosc. 2022;265:120400.
5. Bray F, Ferlay J, Soerjomataram I, Siegel RL, Torre LA, Jemal A. Global cancer statistics 2018: GLOBOCAN estimates of incidence and mortality worldwide for 36 cancers in 185 countries. CA Cancer J Clin. 2018;68(6):394–424.
6. Beslic S, Zukic F, Milisic S. Percutaneous transthoracic CT guided biopsies of lung lesions; fine needle aspiration biopsy versus core biopsy. Radiol Oncol. 2012;46(1):19–22.
7. Zhang Z, Zou H, Yuan A, Jiang F, Zhao B, Liu Y, Chen J, Zuo M, Gong L. A single enhanced dual-energy CT scan may distinguish lung squamous cell Carcinoma from Adenocarcinoma during the venous phase. Acad Radiol. 2020;27(5):624–9.
8. MacMahon H, Naidich DP, Goo JM, Lee KS, Leung ANC, Mayo JR, Mehta AC, Ohno Y, Powell CA, Prokop M, Rubin GD, Schaefer-Prokop CM, Travis WD, Van Schil PE, Bankier AA. Guidelines for management of Incidental Pulmonary nodules detected on CT images: from the Fleischner Society 2017. Radiology. 2017;284(1):228–43.
9. Saijo N, Niitani H, Tominaga K, Eguchi K, Koketsu H, Fujino T, Ishikawa S. Comparison of survival in nonresected well differentiated and poorly differentiated adenocarcinoma of the lung. J Cancer Res Clin Oncol. 1980;97(1):71–9.
10. Baxa J, Vondrakova A, Matouskova T, Ruzickova O, Schmidt B, Flohr T, Sedlmair M, Ferda J. Dual-phase dual-energy CT in patients with lung cancer: assessment of the additional value of iodine quantification in lymph node therapy response. Eur Radiol. 2014;24(8):1981–8.
11. Yoon SH, Park CM, Park SJ, Yoon JH, Hahn S, Goo JM. Tumor heterogeneity in Lung Cancer: Assessment with Dynamic contrast-enhanced MR Imaging. Radiology. 2016;280(3):940–8.
12. Kokavec A, Laba J. A case of MRI-Negative Leptomeningeal Disease from Non-small Cell Lung Cancer. Cureus. 2024;16(3):e56727.
13. Bing X, Wang N, Li Y, Sun H, Yao J, Li R, Li Z, Ouyang A. The value of dual-energy computed tomography-based Radiomics in the evaluation of interstitial fibers of Clear Cell Renal Carcinoma. Technol Cancer Res Treat. 2024;23:15330338241235554.
14. Abu-Omar A, Murray N, Ali IT, Khosa F, Barrett S, Sheikh A, Nicolaou S, Tamburrini S, Iacobellis F, Sica G, Granata V, Saba L, Masala S, Scaglione M. Utility of dual-energy computed Tomography in Clinical Conundra. Diagnostics (Basel) 14(7) (2024).
15. Singla N, Joshi M, Amerasekera S, Choudhary S. Applications of dual-energy CT in acute musculoskeletal and trauma imaging-a review. Skeletal Radiol (2024).
16. Feng QX, Zhu ZN, Li Q, Liu XS. Dual-energy CT quantitative parameters to evaluate occult peritoneal metastasis in advanced gastric cancer preoperatively, Abdom Radiol (NY) (2024).
17. Li YX, Li WJ, Xu YS, Jia LL, Wang MM, Qu MM, Wang LL, Lu XD, Lei JQ. Clinical application of dual-layer spectral CT multi-parameter feature to predict microvascular invasion in hepatocellular carcinoma. Clin Hemorheol Microcirc (2024).
18. Fehrenbach U, Kahn J, Boning G, Feldhaus F, Merz K, Frost N, Maurer MH, Renz D, Hamm B, Streitparth F. Spectral CT and its specific values in the staging of patients with non-small cell lung cancer: technical possibilities and clinical impact. Clin Radiol. 2019;74(6):456–66.
19. Li Q, Li X, Li XY, Huo JW, Lv FJ, Luo TY. Spectral CT in Lung Cancer: usefulness of Iodine concentration for evaluation of Tumor Angiogenesis and Prognosis. AJR Am J Roentgenol. 2020;215(3):595–602.
20. Wang G, Zhang C, Li M, Deng K, Li W. Preliminary application of high-definition computed tomographic Gemstone Spectral Imaging in lung cancer. J Comput Assist Tomogr. 2014;38(1):77–81.
21. Bousse A, Kandarpa VSS, Rit S, Perelli A, Li M, Wang G, Zhou J, Wang G. Systematic review on Learning-based spectral CT. IEEE Trans Radiat Plasma Med Sci. 2024;8(2):113–37.
22. Ng SP, Cardenas CE, Elhalawani H, Pollard C 3rd, Elgohari B, Fang P, Meheissen M, Guha-Thakurta N, Bahig H, Johnson JM, Kamal M, Garden AS, Reddy JP, Su SY, Ferrarotto R, Frank SJ, Brandon Gunn G, Moreno AC, Rosenthal DI, Fuller CD, Phan J. Comparison of tumor delineation using dual energy computed tomography versus magnetic resonance imaging in head and neck cancer re-irradiation cases. Phys Imaging Radiat Oncol. 2020;14:1–5.
23. Liu JX, Zhang Y, Zhou H, Zhao YJ, Dai YS, Zuo ZW, Wang JN, Yin XP. Optimizing the image quality of peripancreatic blood vessels through the clinical application of single-energy spectral computed tomography (CT) imaging. Quant Imaging Med Surg. 2024;14(6):3951–8.
24. Karcaaltincaba M, Aktas A. Dual-energy CT revisited with multidetector CT: review of principles and clinical applications. Diagn Interv Radiol. 2011;17(3):181–94.
25. Mu R, Meng Z, Guo Z, Qin X, Huang G, Yang X, Jin H, Yang P, Deng M, Zhang X, Zhu X. Diagnostic value of dual-layer spectral detector CT in differentiating lung adenocarcinoma from squamous cell carcinoma. Front Oncol. 2022;12:868216.
26. Wang P, Tang Z, Xiao Z, Wu L, Hong R, Wang J. Dual-energy CT for differentiating early glottic squamous cell carcinoma from chronic inflammation and leucoplakia of vocal cord: comparison with simulated conventional 120 kVp CT, Clin Radiol 76(3) (2021) 238 e17-238 e24.
27. Yoon J, Choi Y, Jang J, Shin NY, Ahn KJ, Kim BS. Preoperative assessment of cervical lymph node metastases in patients with papillary thyroid carcinoma: incremental diagnostic value of dual-energy CT combined with ultrasound. PLoS ONE. 2021;16(12):e0261233.
28. Xie X, Liu K, Luo K, Xu Y, Zhang L, Wang M, Shen W, Zhou Z. Value of dual-layer spectral detector computed tomography in the diagnosis of benign/malignant solid solitary pulmonary nodules and establishment of a prediction model. Front Oncol. 2023;13:1147479.
29. Zhong LJ, Yu N, Zhou XJ, Fu LZ, Zhou DQ, Wang Y, Yan M. Differentiating between pulmonary adenocarcinoma and squamous cell carcinoma by spectral CT volumetric quantitative analysis: a comparative study with conventional spectral analysis. J Thorac Dis. 2023;15(2):679–89.
30. Mo H, Huang R, Wei X, Huang L, Huang J, Chen J, Qin M, Lu W, Yu X, Liu M, Ding K. Diagnosis of metastatic lymph nodes in patients with Hepatocellular Carcinoma using dual-energy computed Tomography. J Comput Assist Tomogr. 2023;47(3):355–60.
31. Gao W, Zhang Y, Dou Y, Zhao L, Wu H, Yang Z, Liu A, Zhu L, Hao F. Association between extramural vascular invasion and iodine quantification using dual-energy computed tomography of rectal cancer: a preliminary study. Eur J Radiol. 2023;158:110618.
32. Zheng M. Classification and Pathology of Lung Cancer. Surg Oncol Clin N Am. 2016;25(3):447–68.
33. Winkelmann MT, Gassenmaier S, Walter SS, Artzner C, Nikolaou K, Bongers MN. Differentiation of Hamartomas and malignant lung tumors in single-phased dual-energy computed Tomography. Tomography. 2024;10(2):255–65.

34. Gaudreault M, Bucknell N, Woon B, Kron T, Hofman MS, Siva S, Hardcastle N. Dose-response relationship between Radiation Therapy and loss of lung perfusion comparing Positron Emission Tomography and Dual-Energy Computed Tomography in Non-small Cell Lung Cancer. Int J Radiat Oncol Biol Phys. 2024;118(4):1135–43.

Publisher's note